JCTC Journal of Chemical Theory and Computation

Article

pubs.acs.org/JCTC

Conical Intersection Optimization Using Composed Steps Inside the ONIOM(QM:MM) Scheme: CASSCF:UFF Implementation with Microiterations

Sergi Ruiz-Barragan,[†,§] Keiji Morokuma,[‡] and Lluís Blancafort*[,†]

[†]Institut de Química Computacional i Catàlisis and Departament de Química, Universitat de Girona, Campus de Montilivi, 17071 Girona, Spain

[‡]Fukui Institute for Fundamental Chemistry, Kyoto University, Kyoto 606-8103, Japan

Supporting Information

ABSTRACT: Three algorithms for optimization of minimum energy conical intersections (MECI) are implemented inside an ONIOM(QM:MM) scheme combined with microiterations. The algorithms follow the composed gradient (CG), composed gradient−composed steps (CG-CS), and double Newton−Raphson-composed step (DNR-CS) schemes developed previously for purely QM optimizations. The CASSCF and UFF methods are employed for the QM and MM calculations, respectively. Conical intersections are essential to describe excited state processes in chemistry, including biological systems or functional molecules, and our approach is suitable for large molecules or systems where the excitation is well localized on a fragment that can be treated at the CASSCF level. The algorithms are tested on a set of 14 large hydrocarbons composed of a medium-sized chromophore (fulvene, benzene, butadiene, and hexatriene) derivatized with alkyl substituents. Thanks to the microiteration technique, the number of steps required to optimize the MECI of the large molecules is similar to the one needed to optimize the unsubstituted chromophores at the QM level. The three tested algorithms have a similar performance, although the CG-CS implementation is the most efficient one on average. The implementation can be straightforwardly applied to ONIOM(QM:QM) schemes, and its potential is further demonstrated locating the MECI of diphenyl dibenzofulvene (DPDBF) in its crystal, which is relevant for the aggregation induced emission (AIE) of this molecule. A cluster of 12 molecules (528 atoms) is relaxed during the MECI optimization, with one molecule treated at the QM level. Our results confirm the mechanistic picture that AIE in DPDBF is due to the packing of the molecules in the crystal. Even when the molecules surrounding the excited molecule are allowed to relax, the rotation of the bulky substituents is hindered, and the conical intersection responsible for radiationless decay in solution is not accessible energetically.

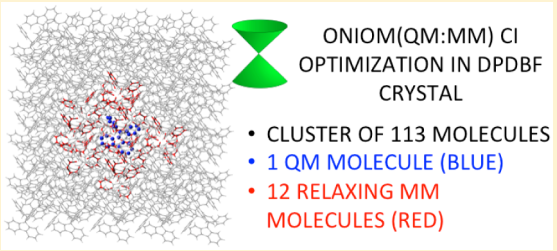

INTRODUCTION

Conical intersections (CIs) are fundamental structures for photochemistry and photophysics,[1−6] where the energy difference between two or more electronic states is zero. These structures can provide rapid deactivation pathways from excited states to lower ones when they are accessible in energy. The importance of conical intersections has been well established in spectroscopy,[7] photochemical organic reactions,[8−12] biological systems,[13−18] or applications such as photochromic systems[19,20] or luminescent materials.[21]

CIs are not isolated points on the potential energy surface (PES) but form seams of intersection.[22−24] The seams are (N-2)-dimensional subspaces where the degeneracy remains, with N being the number of degrees of freedom of the PES. The location of the minimal energy conical intersection (MECI) structure is a key step in computational photochemistry studies[25] since in many cases it provides a first mechanistic interpretation of the process of interest and serves as a doorway for more refined analyses that take the full nature of the seam into account. For this reason, several CI optimization algorithms have been developed in the last decades to locate MECIs in small to medium-sized molecules, both in the gas phase and in solution.[26−38] Here, we focus on large molecules and systems where the environment has a substantial influence on the excited state behavior, such as biological systems or molecules in solution or in crystals. To treat these systems, we present the implementation of three CI optimization methods within the ONIOM scheme.[39−46] The ONIOM scheme is a versatile tool to study such systems since it can be used in hybrid quantum mechanics/molecular mechanics (QM:MM) or QM:QM schemes; it can also be used to study large molecules, dividing the molecule into different fragments, or to study environmental effects. Our goal is to derive an efficient CI optimization scheme for all these cases.

The algorithms we have implemented are based on projected gradients (see the Theoretical Basis section) and combine efficiency with straightforward implementation. They are based

Received: January 4, 2015
Published: March 2, 2015

DOI: 10.1021/acs.jctc.5b00004
J. Chem. Theory Comput. 2015, 11, 1585−1594

on the composed gradient (CG),[27] composed step (CS),[33] and double Newton−Raphson (DNR)[37] methods. The most common one is the CG algorithm implemented in the Gaussian program, and the CS and DNR algorithms are improved versions developed in the last few years. The implementation of the CG algorithm within ONIOM was described some years ago;[47] here, we implement a slightly different CG scheme in ONIOM together with the CS and DNR methods and compare the performance of the three. The algorithms are tested on a set of large molecules. All cases are treated at the QM:MM level, combining the complete active space self-consistent field (CASSCF) method with the universal force field (UFF).[48] As we explain below in detail, the optimizations are carried out using microoptimizations to maximize the efficiency.[49] The set is based on fulvene,[8] benzene,[50] and butadiene,[51] which have well-known CIs. It includes 13 derivatives with bulky substituents and the CI corresponding to the ring opening of ergosterol.[52] On average, the most efficient implementation is the combination of CG and CS. To show the potential of our approach to treat environment effects, we have also considered the diphenyl dibenzofulvene (DPDBF) molecule in its crystal (see Scheme 1), which shows aggregation-induced emission.[53] In the gas phase, DPDBF has an energetically accessible CI. The crystal packing is a structural restraint that raises the energy of the CI compared to that of the gas phase, and relaxation of the molecules that surround the excited molecule does not stabilize the CI significantly. This explains the appearance of fluorescence in the aggregate phase.

Scheme 1

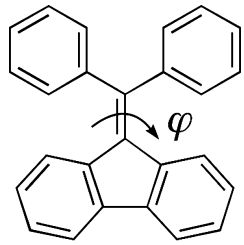

DPDBF

THEORETICAL BASIS

Conical Intersection Optimization with Projected Gradients. The CI minimization conditions for two electronic states are

$$\Delta\varepsilon = 0$$
$$\mathbf{g}_{IS} = 0 \tag{1a,b}$$

where $\Delta\varepsilon$ is the energy difference between the two states and g_{IS} the gradient inside the seam space, the so-called intersection space (IS). The complementary space of the IS is the branching space (BS), which is formed by the modes which break the degeneracy.[6,22] In the first order approximation, the BS is formed by two modes:

$$\mathbf{x}_1 = \nabla(\varepsilon_i - \varepsilon_j)$$
$$\mathbf{x}_2 = \nabla\langle\psi_i|\hat{H}|\psi_j\rangle \tag{2a,b}$$

where $\mathbf{x}_1$ is the gradient difference vector and $\mathbf{x}_2$ the interstate coupling vector, and ε_i and ψ_i are the energy and the electronic wave function of the electronic state i, respectively. It is possible to project the gradient of the system outside the BS with a projector, using the first order BS:

$$\mathbf{P} = \mathbf{I} - \hat{\mathbf{x}}_1\hat{\mathbf{x}}_1^{\mathrm{T}} - \hat{\mathbf{x}}_2\hat{\mathbf{x}}_2^{\mathrm{T}} \tag{3}$$

where $\hat{\mathbf{x}}_i$ stands for a normalized vector. The IS gradient is obtained projecting the gradient of the degenerate states:

$$\mathbf{g}_{IS} = \mathbf{P}\mathbf{g}_i = \mathbf{P}\mathbf{g}_j \tag{4}$$

The projected gradient does not change the energy difference to first order. In this work, we use projected gradient based algorithms, where the projected gradient drives the MECI optimizations in combination with the quasi-Newton−Raphson method. The first algorithm of this type, and one of the most widely used ones, is the CG one,[27] implemented in Gaussian.[54] The CG has the following form:

$$\mathbf{g}^{CG} = \mathbf{g}_{IS} + \mathbf{f} = \mathbf{g}_{IS} + 2\Delta\varepsilon\mathbf{x}_1 \tag{5}$$

where $\mathbf{f}$ plays the role of a penalty function to reach degeneracy. The two parts of the CG can be considered as the two conditions of the MECI: the penalty function gets to zero when the algorithm reaches degeneracy, and the projected gradient gets to zero when the algorithm reaches the minimum inside the IS. The optimization steps are obtained following the quasi-Newton−Raphson method:

$$\Delta\mathbf{q}^{CG} = \mathbf{H}^{-1}\mathbf{g}^{CG} \tag{6}$$

The CG algorithm is inefficient because the Hessian, obtained with the composed gradient and the Broyden−Fletcher−Goldfarb−Shanno (BFGS) update procedure,[55] is not well-defined since the gradient is a sum of different terms. This slows down the optimization because the degeneracy can be lost due to the ill-defined Hessian.[33]

The CS algorithm[33] was derived to improve the definition of the Hessian. It is similar to the one derived in a Lagrangian formalism in ref 28. The main idea is to separate the displacements in two different steps, one for each space (IS and BS), to fulfill the two conditions of the MECI:

$$\Delta\mathbf{q} = \Delta\mathbf{q}_{IS} + \Delta\mathbf{q}_{BS} \tag{7}$$

The IS step is a Newton−Rapshon minimization inside the IS using the projected gradient

$$\Delta\mathbf{q}_{IS} = \mathbf{H}_{IS}^{-1}\mathbf{g}_{IS} \tag{8}$$

In this case, the Hessian ($\mathbf{H}_{IS}$) is the Hessian inside the IS,[56] obtained with the BFGS update using $\mathbf{g}_{IS}$. The intersection space Hessian does not change the energy difference, and the convergence is improved with respect to the CG case. The BS step is used to reach the degeneracy, using a first order approximation for the energy difference.

$$\Delta\mathbf{q}_{BS} = -\Delta\varepsilon\frac{1}{|\mathbf{x}_1|}\hat{\mathbf{x}}_1 \tag{9}$$

The first order approximation has a poor approach to the degeneracy because the steps are forced to go in the direction of $\mathbf{x}_1$, and the second-order degeneracy lifting effects along other modes, which can be important, are ignored. In this respect, the CG algorithm has a more efficient approach to the seam when $\mathbf{f}$ dominates over $\mathbf{g}_{IS}$ (see eq 5). For this reason, in

DOI: 10.1021/acs.jctc.5b00004
J. Chem. Theory Comput. 2015, 11, 1585−1594

the most efficient implementation the two algorithms were combined in a hybrid CG-CS algorithm, where the CG and CS algorithms are used in the initial and final steps of the optimization, respectively. The CG-CS implementation exploits the best properties of each algorithm.

Recently, the DNR algorithm has been proposed[37] as a development of the CG and CS algorithms with an improved approach to the seam. DNR follows a CS scheme where each step is composed by two steps based on a quasi-Newton−Raphson optimization for the two conditions of the MECI:

$$\begin{aligned}\Delta\mathbf{q} &= \Delta\mathbf{q}_{IS} + \Delta\mathbf{q}_{BS}\\ \Delta\mathbf{q}_{IS} &= \mathbf{H}_{IS}^{-1}\mathbf{g}_{IS}\\ \Delta\mathbf{q}_{BS} &= \mathbf{H}_{BS}^{-1}\mathbf{g}_{BS}\\ \mathbf{g}_{IS} &= \mathbf{P}\mathbf{g}_{i}\\ \mathbf{g}_{BS} &= 2(\Delta\varepsilon)^2\hat{\mathbf{x}}_1\end{aligned} \tag{10a−e}$$

where $\mathbf{g}_{BS}$ is the gradient of the $(\Delta\varepsilon)^2$ function and $\mathbf{H}_{BS}$ the Hessian of the BS, defined as the derivative of $\mathbf{g}_{BS}$ and obtained with the BFGS update. The two gradients fulfill the two conditions of the MECI, minimum energy inside the IS and degeneracy. In this case, the degeneracy is reached more quickly than in the CG case and is not lost because the Hessians are well described.

ONIOM Scheme. ONIOM is a multilayer scheme based on extrapolation that combines different levels of calculation for a given system.[39−46] In the simplest, two-layer case, the energy is obtained from three independent calculations using high and low level methods: one for the *real* system that contains all atoms, and two for the *model* system that contains, in the present case, the part of the system directly involved in the excitation:

$$\varepsilon^{ONIOM} = \varepsilon^{high}_{model} + \varepsilon^{low}_{Real} - \varepsilon^{low}_{model} \equiv \varepsilon^{QM}_{model} + \varepsilon^{MM}_{Real} - \varepsilon^{MM}_{model} \tag{11}$$

The gradient of the energy function is the sum of the gradients of the three energy terms. In this work, we use ONIOM as an extrapolative QM:MM scheme (third part of eq 11), with CASSCF as the QM level and UFF[48] as the MM one. The MM atoms have no partial charges because the UFF parameters were obtained without charges, and the electrostatic interaction between the model region and the rest of the system is treated implicitly at the MM level through parametrization. This simplifies the implementation because there are no interaction terms between the charges of the QM and MM regions. Moreover, in this work we deal with hydrocarbons, where this contribution can be assumed to be small, anyway. Our implementation is also valid for other QM:MM schemes with no embedding or purely extrapolative QM:QM schemes. However, the extension to other force fields including atomic charges and electronic embedding will require some modifications, as discussed in the Conclusions.

Choosing a correct model is fundamental in the ONIOM scheme. However, in the present examples this choice is straightforward because the electronic excitation is well localized in a fragment of the molecule. In the cases where the division between layers requires cutting bonds, ONIOM employs the link atom (LA) approach. The atoms of the low-level layer connected to the atoms of the high-level layer, called linked atom hosts (LAHs), are replaced by the LAs, which in turn are included in the model system. The position of the LA depends on the coordinates of the atoms that form the real bond:

$$\mathbf{q}_{LA} = \mathbf{q}_{LAC} + k(\mathbf{q}_{LAH} - \mathbf{q}_{LAC}) \tag{12}$$

where q_{LA}, q_{LAC}, and q_{LAH} are the position of the LA, the LAH, and the link atom connection (LAC). k is a scale factor and depends on the elements that form the bond. Usually, hydrogen atoms are used as LAs. This transformation makes a Jacobian transformation of the model system gradients necessary to make them consistent with the gradients of the real system:

$$\mathbf{g}^{ONIOM} = \mathbf{g}^{QM}_{model}\mathbf{J} + \mathbf{g}^{MM}_{real} - \mathbf{g}^{MM}_{model}\mathbf{J} \tag{13}$$

The optimization process can be made more efficient with the microiteration scheme.[49] In this case, the atoms which do not affect the energy of the model system are optimized completely for every optimization step of the model (note that this separation is not equivalent to the one between low- and high-level atoms; see more details in ref 49). Therefore, the ONIOM optimization step is divided into two parts, a sum of steps for the atoms involved in the microiterations ($\Delta\mathbf{q}^l$) and a step for the remaining atoms ($\Delta\mathbf{q}^m$):

$$\Delta\mathbf{q}^{ONIOM} = \begin{pmatrix}\Delta\mathbf{q}^m\\ 0\end{pmatrix} + \begin{pmatrix}0\\ \sum\Delta\mathbf{q}^l\end{pmatrix} \tag{14}$$

The step for the high-level part is usually a quasi Newton−Raphson step. This procedure speeds up the overall optimization because the cost of calculating the MM gradients is only a fraction of that of calculating the QM ones.

Excited States and MECI Optimization with ONIOM. The calculation of excited states with ONIOM is greatly simplified if one assumes that the excitation is localized in the high-level moiety. This is the case for the systems that we consider here. This allows the use of standard molecular mechanics methods for the low level since this level does not have to describe the excitation. This is also the assumption made in the previous work on MECI optimization with ONIOM,[47] and we follow this work for the derivation of the BS vectors and the IS gradient. In this approximation, the energy of state i is defined as

$$\varepsilon_i^{ONIOM} = \varepsilon^{High}_{i,model} + \varepsilon^{Low}_{real} - \varepsilon^{Low}_{model} \tag{15}$$

Considering that there are no QM:MM electrostatic cross-terms, the relative excitation energy or S_i/S_j energy gap of the real system is equal to that of the model:

$$\Delta\varepsilon_{real} = \Delta\varepsilon_{model} \tag{16}$$

For simplicity, we refer to the energy gap as $\Delta\varepsilon$. Similarly, the gradients of the states are

$$\mathbf{g}_i^{ONIOM} = \mathbf{g}^{high}_{i,model}\mathbf{J} + \mathbf{g}^{low}_{real} - \mathbf{g}^{low}_{model}\mathbf{J} \tag{17}$$

From this, it follows that the first order BS vectors can be obtained applying the Jacobian transformation to the BS vectors from the high-level calculation:

$$\begin{aligned}\mathbf{x}_1^{ONIOM} &= \mathbf{x}^{high}_{1,model}\mathbf{J}\\ \mathbf{x}_2^{ONIOM} &= \mathbf{x}^{high}_{2,model}\mathbf{J}\end{aligned} \tag{18}$$

DOI: 10.1021/acs.jctc.5b00004
J. Chem. Theory Comput. 2015, 11, 1585−1594

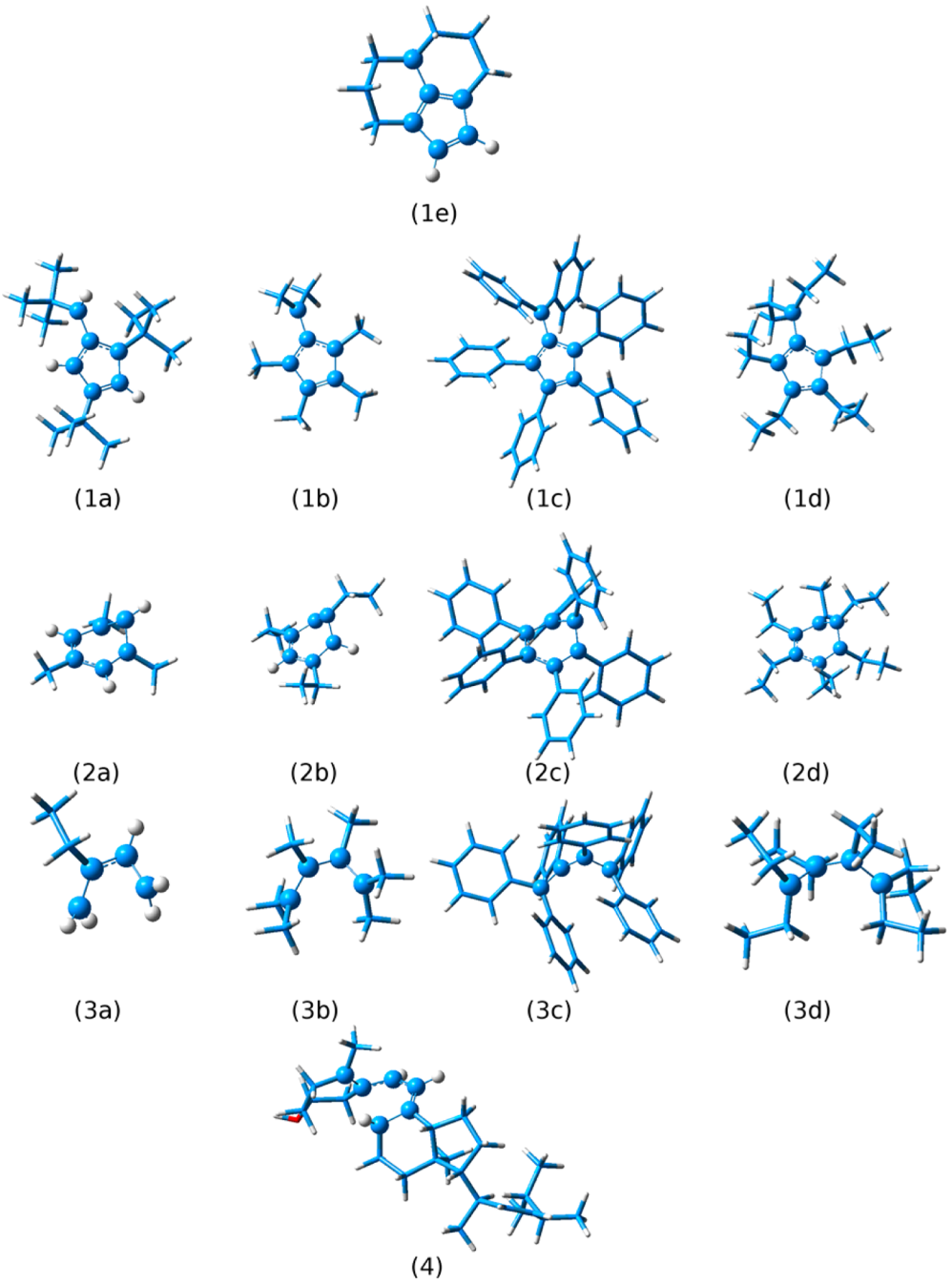

Figure 1. Test set of 14 molecules used for the MECI optimizations with the CG, CG-CS, and DNR-CS algorithms.

For the MECI optimization, the IS gradient can be obtained using the projector built with the ONIOM BS vectors $\mathbf{x}_1^{ONIOM}$ and $\mathbf{x}_2^{ONIOM}$ (see eq 3):

$$\mathbf{g}_{IS}^{ONIOM} = \hat{\mathbf{P}}^{ONIOM}\mathbf{g}_i^{ONIOM} \tag{19}$$

In our approximation, using mechanical embedding and microoptimizations, only the step for the model part in eq 14 has to be changed. The model steps for the three algorithms described previously are

ONIOM CG:

$$\Delta\mathbf{q}^m = -\mathbf{H}^{-1}(\mathbf{g}_{IS}^{ONIOM} + 2\Delta\varepsilon\hat{\mathbf{x}}_1^{ONIOM}) \tag{20}$$

ONIOM CS:

$$\Delta\mathbf{q}_{IS}^m = -\mathbf{H}_{IS}^{-1}\mathbf{g}_{IS}^{ONIOM}$$
$$\Delta\mathbf{q}_{BS}^m = -\frac{\Delta\varepsilon}{|\mathbf{x}_1^{ONIOM}|}\hat{\mathbf{x}}_1^{ONIOM} \tag{21}$$

ONIOM DNR:

$$\Delta\mathbf{q}_{IS}^m = -\mathbf{H}_{IS}^{-1}\mathbf{g}_{IS}^{ONIOM}$$
$$\Delta\mathbf{q}_{BS}^m = -\mathbf{H}_{BS}^{-1}\mathbf{x}_1^{ONIOM} \tag{22}$$

where the gradients are written with the ONIOM formulation, and the Hessians are obtained with the BFGS update. In this implementation, the microiteration steps are independent from

DOI: 10.1021/acs.jctc.5b00004
J. Chem. Theory Comput. 2015, 11, 1585−1594

the MECI optimization step and do not change with respect to standard ONIOM.

COMPUTATIONAL DETAILS

The MECI projected gradient algorithms have been implemented in the Gaussian program.[54] All practical issues commented in ref 37 have been implemented in the same way in this work. In particular, the projection step (eq 19) is carried out in redundant coordinates in all cases. This is the main difference with respect to ref 47, where the projection is done in Cartesians. In the CG-CS implementation, the optimization starts with the CG algorithm and switches to CS when $\Delta\varepsilon$ falls below a threshold of 0.005 hartree. In the DNR-CS case, the optimization starts with the DNR algorithm and switches to CS when a step leads to a large increase in the S_1/S_0 energy gap near the seam. The implementations work also without microiterations, but we only show the results of the more efficient microiteration scheme.

The three MECI algorithms have been tested with a set of 14 molecules shown in Figure 1. The test set consists of 13 derivatives of fulvene, benzene, and 1,3-butadiene, substituted with alkyl and phenyl groups. In all cases, the excitation is well localized on the fulvene, benzene, or butadiene chromophore. This is also the case for the phenyl-substituted molecules because the phenyl rings are rotated with respect to the chromophore, and the electronic coupling is weak. The chromophores form the high-level moiety and the substituents the low-level one. The test set also includes the CI corresponding to the ring opening of ergosterol, an analogue of which was tested in the previous implementation of an ONIOM MECI algorithm.[47] In this molecule, the high-level region is formed by the hexatriene chain shown in Figure 1. All optimizations start near the minimum of S_0, releasing any symmetry constraints. The Cartesian coordinates of the initial points, and the optimized structures are given in the Supporting Information.

In the second part of this work, the critical points of DPDBF inside its own crystal are calculated. The real system is composed of 113 DPDBF molecules, where the central molecule is the model system, and the rest is calculated with the low level. To avoid losing the crystal structure, the critical points are optimized allowing only the model system and the first surrounding layer of molecules to relax (11 DPDBF units). The remaining part of the low level layer is kept frozen during the optimization. The starting point for these calculations is the crystal structure from the literature.[57]

The calculations have been carried out at the ONIOM level with state-averaged CASSCF/6-31G** as high level and UFF[48] without partial charges as low-level, using a (6,6) active space for the fulvene, benzene, and ergosterol calculations, a (4,4) one for butadiene, and (12,12) one for DPDBF. All CASSCF gradients have the coupled-perturbed multiconfiguration self-consistent field corrections,[58] except in the case of DPDBF.

RESULTS AND DISCUSSION

Test Set of 14 Molecules. The results of the optimizations for the test set are shown in Table 1. The efficiency of the methods can be assessed from the number of optimization cycles because the evaluation of the CI gradients has the same computational cost in all cases, and the microiterations have a negligible cost. For comparison, we include the optimization results for the unsubstituted cases, carried out at the full QM level with CASSCF. In all cases, the optimization is completed within 60 steps or less, and in several cases, the optimization of the substituted systems needs less steps than that of the unsubstituted molecules, which shows the efficiency of the microiterations scheme in combination with the MECI algorithm. On average, the CG-CS implementation is more efficient than the DNR-CS and CG ones. More in detail, the DNR-CS implementation reaches the MECI in the smallest number of steps in many cases, but in others, it needs a substantially larger number of steps than the other two (molecules **1e**, **2d**, **3c**, and **3d**). This is in contrast to the fully QM implementation, where DNR-CS is the most efficient method.[37] The reasons for this behavior are illustrated with two examples in Figures 2 and 3.

Table 1. Number of Optimization Cycles in MECI Searches with the CG, CG-CS, and DNR-CS Algorithms Inside ONIOM for the Test Set of 14 Molecules and Results for the Unsubstituted Cases

			MECI algorithm		
parent structure	substituents		CG	CG-CS	DNR-CS
fulvene (**1**)	6 × H	(**1**)	26[a]	25[a]	23[a]
	3 × *t*-butyl	(**1a**)	56	32	17
	6 × methyl	(**1b**)	19	19	18
	6 × phenyl	(**1c**)	19	14	25
	6 × ethyl	(**1d**)	23	23	23
	2 × trimethylene	(**1e**)	24	20	29
benzene (**2**)	6 × H	(**2**)	21[a]	21[a]	14[a]
	3 × methyl	(**2a**)	18	18	15
	3 × ethyl	(**2b**)	16	18	16
	6 × phenyl	(**2c**)	32	23	22
	6 × ethyl	(**2d**)	18	19	27
butadiene (**3**)	4 × H	(**3**)	21[a]	16[a]	21[a]
	ethyl	(**3a**)	17	19	24[b]
	6 × methyl	(**3b**)	60	60	47[b]
	6 × phenyl	(**3c**)	29	29[b]	49[b]
	6 × ethyl	(**3d**)	33	33	42
ergosterol		(**4**)	34	33	38
average			28.4	25.7	28.0

[a]Optimization carried out at the fully QM CASSCF level of theory. [b]Optimization leads to a local MECI (*cis*-like geometry) instead of the global MECI (*trans*-like geometry).[51]

In Figure 2, we present the MECI optimization of the fulvene derivative **1a**, where DNR-CS is the most efficient algorithm. The optimizations follow the behavior described in ref 37 for the different algorithms, where the CG gradient repeatedly loses the degeneracy because of the ill-defined Hessian. The CG-CS and DNR-CS implementations do not suffer from this problem, and DNR-CS reaches the seam in less steps than CG-CS, which makes the optimization more efficient.

Figure 3 shows the optimization course for the butadiene derivative **3c**, which carries six phenyl substituents. For this molecule, the DNR-CS algorithm needs more steps than the other two. The graph includes the extrapolated energy (eq 12) and the model energy, calculated at the QM level. The CS algorithm follows the same course as the CG-CS one and is not included in Figure 3. The large number of steps required for the optimization with DNR-CS is due to a sudden rise of the extrapolated energy in steps 5 and 6. This increase is not observed in the model energy and is due to a rise of the MM energy of the real system. The insets of Figure 3 show the

DOI: 10.1021/acs.jctc.5b00004
J. Chem. Theory Comput. 2015, 11, 1585−1594

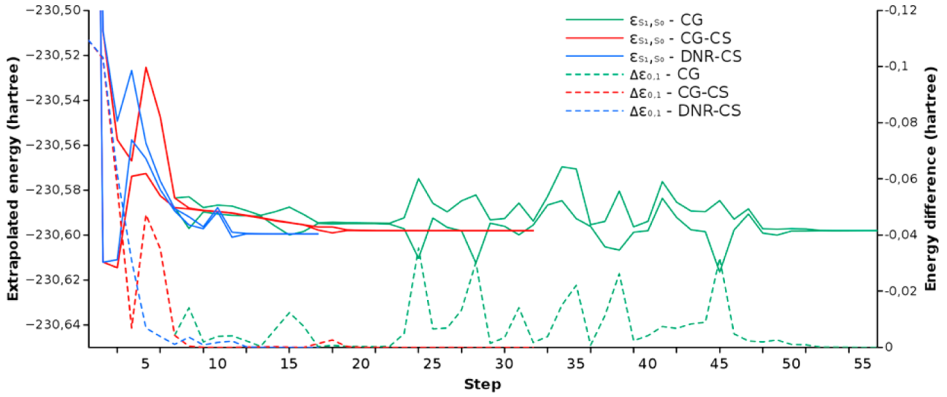

Figure 2. Course of MECI searches with the CG, CG-CS, and DNR-CS algorithms for the fulvene derivative (**1a**) (green, red, and blue lines, respectively). Solid lines: S_1 and S_0 energies (left y axis); dashed lines: $\Delta\varepsilon$ (right y axis). Energies are in hartree.

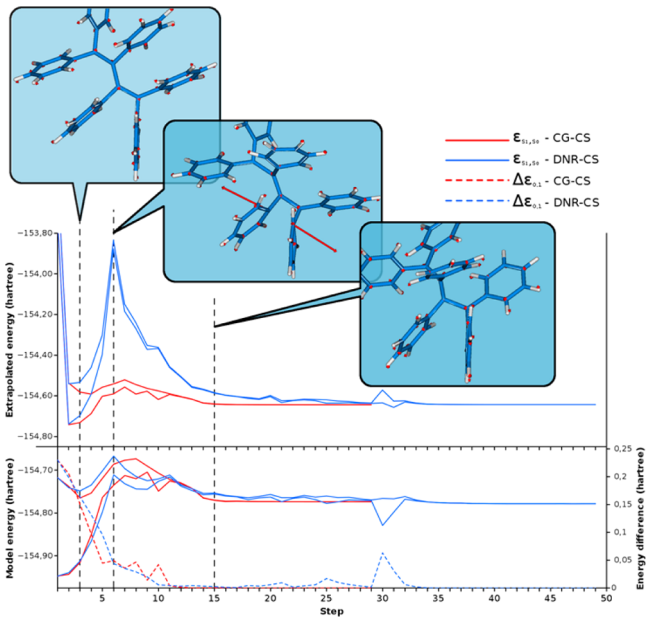

Figure 3. Course of MECI searches with the CG-CS and DNR-CS algorithms for the butadiene derivative (**3a**) (red, and blue lines, respectively). Solid lines, S_1 and S_0 energies (left y axis); dashed lines, $\Delta\varepsilon$ (right y axis). Energies are in hartree. The insets show the structures at steps 3, 6, and 15, and the arrows in the structure at step 6 correspond to the MM forces at that point.

structure of **3a** at steps 3, 6, and 15 of the DNR-CS optimization. The energy increase in step 6 is due to a large steric repulsion between the two phenyl groups. In turn, the approach of the phenyl groups is caused by large $\Delta\mathbf{q}^m$ steps that are dominated by the $\Delta\mathbf{q}^m_{BS}$ term in eq 22. This term is calculated for the model system, where the phenyl groups are replaced by hydrogen atoms, and the large steric repulsion found for the real system is absent. Moreover, the steric repulsion cannot be released during the microiterations because the link atom hosts are frozen during this process, and the extrapolated energy rises significantly. As a result, the energy gradients have large components on the link atom hosts, as shown with arrows in the inset of Figure 3. With the CG and CS-CG methods, the steps in the direction of $\mathbf{x}_1$ are smaller, and the close approach between the substituents does not occur.

Diphenyl Dibenzofulvene. To show the value of our implementation we have also considered the photophysics of diphenyl dibenzofulvene (DPDBF) in its crystal. This molecule shows aggregation induced emission, i.e., it is fluorescent in the condensed phase but not in solution.[53] Our previous work shows that the lack of fluorescence in solution is due to the presence of an energetically accessible CI accessed by rotation of the CC double bond (see the rotation angle φ in Scheme 1). This intersection is not accessible in the solid phase because the rotation of the phenyl substituents around the CC double bond is blocked.[21] The crystal is modeled with a cluster of 113 DPDBF molecules treated at the UFF level, and one molecule (the central one) at the CASSCF(12,12)/6-31G** level. This is a suitable approach because the excitonic coupling between the different molecules is weak, and the excitation is localized on a single molecule.[21] In our preceding work, the MECI in the crystal was located at the CASSCF:UFF level of theory freezing all the surrounding molecules. With the present approach, the MECI optimization is carried out releasing the first layer of molecules that surround the excited molecule, composed of 11 units. This is made possible by our implementation, coupled with the microiteration technique. Our goal is to assess whether relaxation of the surrounding molecules has an effect on the structure of the optimized MECI and the resulting energy profile for the decay.

The MECI structures obtained with the two approaches are shown in Figure 4, and the energy results are presented in Table 2. The MECI structures are very similar and are characterized by a large stretch of the CC bond to 1.75 Å and a nearly planar CC double bond. This is in contrast with the MECI in the gas phase, where the CC bond is twisted by

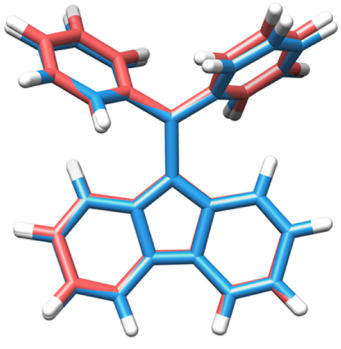

Figure 4. Overlay of the MECIs of DPDBF optimized in the crystal, freezing all surrounding molecules (in red) and allowing relaxation of the first surrounding layer (in blue).

DOI: 10.1021/acs.jctc.5b00004
J. Chem. Theory Comput. 2015, 11, 1585−1594

Table 2. ONIOM (CASSCF:UFF) Extrapolated Energies for the Structures along the Decay Path for DPDBF in Its Crystal (Energies in eV Relative to the Ground State Energy of S_0-Min)

	fully frozen environment[a]		relaxed surrounding layer[b]	
structure	S_0	S_1	S_0	S_1
S_0-Min	0.00	4.42	0.00	4.39
S_1-Min	1.29	3.84	1.49	3.94
MECI	5.71	5.71	5.78	5.78

[a]Structures optimized freezing all non-QM molecules. [b]Structures optimized allowing the first layer around the QM molecule to relax.

approximately 90°. The main differences between the two MECI in the crystal are found in the rotation of the phenyl substituents (see Figure 4). Overall, the packing of the molecules in the crystal is so tight that the release of the surrounding molecules in the optimization has only a small effect on the structure of the MECI.

Turning to the relative energies, the profiles obtained in the crystal with the two approaches are similar. In both cases, the energy of the MECI lies higher in energy than the vertical excitation, which explains the emission observed in the condensed phase and is in agreement with our previous calculations.[21] The comparison of the two approaches shows that the relative energies of the S_1 minimum and the MECI are somewhat increased when the first layer is allowed to relax as compared to the fully frozen environment. This is due to the fact that the structure of the ground-state is also reoptimized in the free first layer case, which leads to a larger decrease of its energy compared to that of the other two structures. Compared to the frozen crystal, the ground-state minimum is more stabilized because UFF is a ground state method. In terms of absolute energy, the relaxation of the first layer provides a stabilization of about 0.69 hartree, but the effect on the position of the single atoms is small. This is shown in Figure 5 by comparing the crystal structure with that resulting from optimization of the first layer.

CONCLUSIONS

Three projected-gradient algorithms for the location of MECIs, namely, CG, CG-CS, and DNR-CS, are implemented inside the ONIOM scheme and combined with microiterations. The implementation is suitable to locate MECI for large molecules where the chromophore is localized on a fragment of the molecule that can be treated at the CASSCF level. It is also appropriate for systems where the interaction between the chromophore and the rest of the system is dominated by steric effects, and charge interactions can be neglected. The algorithms are tested with a set of 14 hydrocarbons, derivatives of fulvene, benzene, butadiene, and hexatriene with bulky substituents. The MECIs are located in a similar number of steps compared to the steps needed to optimize the MECI in the unsubstituted molecules, at the fully QM level. This shows the efficiency of the implementation. Regarding the different algorithms, the most efficient one on average is the CG-CS one. The DNR-CS algorithm is more efficient in several cases, similar to our previous implementation at the fully QM level, but it has problems with very bulky substituents because large steps in the branching space, which aim to reach energy degeneracy, cause steric clashes between the substituents. In these cases, the CG-CS algorithm is more efficient. Our method

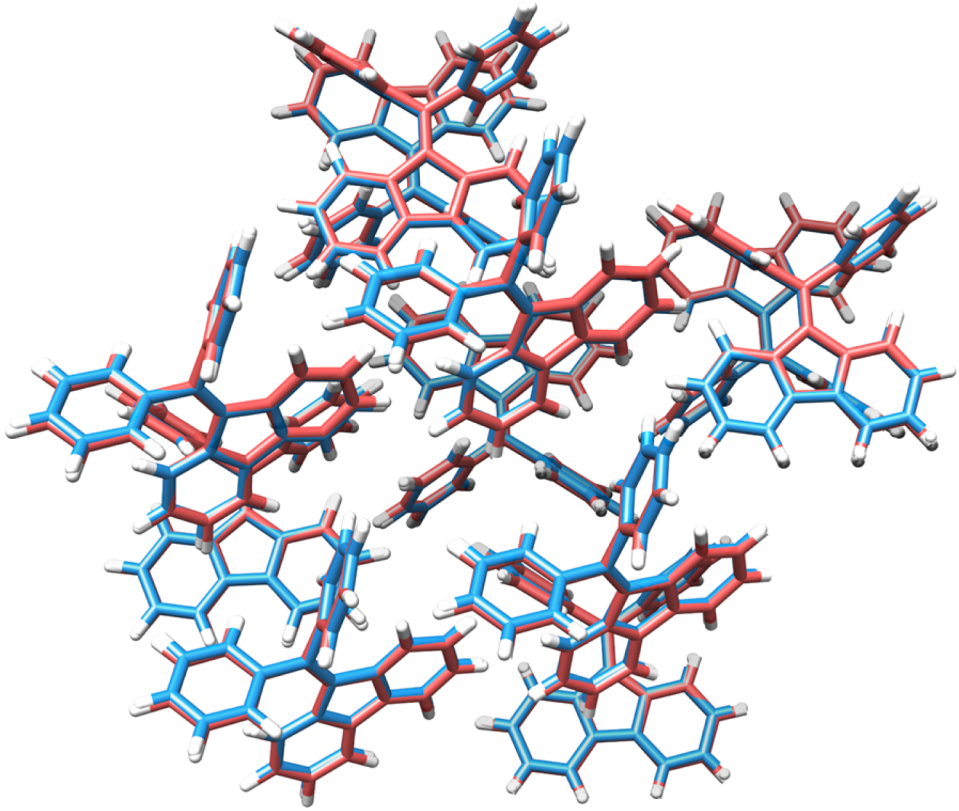

Figure 5. Overlay of the crystal structure (in blue) and the ONIOM(CASSCF:UFF) optimized S_0 structure (in red) for the DPDBF active center and the first layer of surrounding molecules.

DOI: 10.1021/acs.jctc.5b00004
J. Chem. Theory Comput. 2015, 11, 1585−1594

can also be used to locate conical intersections in crystals of organic molecules where the excitation is centered on a single molecule, as shown here for the DPDBF case. In particular, our implementation allows to relax a part of the crystal molecules during the MECI optimization by using the microiteration technique. In DPDBF, the packing of the molecules is so tight that releasing the surrounding molecules has only a small effect on the structures and the resulting mechanism, and future work will show if this is a general feature of organic crystals.

Our next goal is to adapt this scheme to the treatment of the photophysics and photochemistry of systems where electrostatic interactions between the chromophore and the environment are important, such as molecules in solution or biological systems like proteins or DNA. This will require the use of partial atomic charges, and the algorithms will be implemented for the EE case. From the technical point of view, the clue is to treat the microiteration steps correctly. In the present implementation, the displacements of the low-level atoms do not affect the CI conditions, and the microiterations are carried out in the same way as a standard ONIOM optimization. In the EE case, the projection of the gradient along the branching space vectors (eq 19) has to be carried out also during the microiteration steps. We also aim to combine the CI optimization algorithms with the polarizable QM/MM approach recently implemented for CASSCF.[59] The systems mentioned above are also flexible, and it can be anticipated that the study of the CIs will also require to sample the conformational space. This can be achieved by sampling representative conformations from ground state molecular dynamics and locating the MECI from different initial conformations. This approach will provide a good starting point to understand the excited state dynamics that can, eventually, be completed by computing the actual dynamics. This will be the subject of future work.

■ ASSOCIATED CONTENT

Supporting Information

Cartesian coordinates of the MECI and optimization initial points. This material is available free of charge via the Internet at http://pubs.acs.org.

■ AUTHOR INFORMATION

Corresponding Author

*E-mail: lluis.blancafort@udg.edu.

Present Address

[§](S.R.-B.) Japan Atomic Energy Agency, Kashiwanoha Campus, Tokyo University, 178-4-4, Wakashiba, Kashiwa, Chiba 277-0871, Japan.

Notes

The authors declare no competing financial interest.

■ ACKNOWLEDGMENTS

This work has been supported by grant CTQ2011-26573 from the Spanish Ministerio de Economía y Competividad (MINECO), 2014SGR1202 from the Catalan Agència de Gestió d'Ajuts Universitaris i de Recerca (AGAUR), UNGI10-4E-801 from the Spanish Ministerio de Ciencia e Innovación (MICINN) and the European Fund for Regional Development, and the Xarxa de Referència en Química Teòrica i Computacional de Catalunya from AGAUR. S.R.-B. thanks the MINECO for grant BES-2009-029177 and a travel grant EEBB-I-12-04604.

■ REFERENCES

(1) Klessinger, M.; Michl, J. *Excited States and Photochemistry of Organic Molecules*; VCH Publishers, Inc.: New York, 1995.

(2) Bernardi, F.; Olivucci, M.; Robb, M. A. Potential energy surface crossings in organic photochemistry. *Chem. Soc. Rev.* **1996**, *25*, 321−328.

(3) Yarkony, D. R. Diabolical conical intersections. *Rev. Mod. Phys.* **1996**, *68*, 985−1013.

(4) *Conical Intersections: Electronic Structure, Dynamics & Spectroscopy*; Domcke, W., Yarkony, D. R., Köppel, H., Eds.; World Scientific: Singapore, 2004.

(5) *Conical Intersections: Theory, Computation and Experiment*; Domcke, W., Yarkony, D. R., Köppel, H., Eds.; World Scientific: Singapore, 2011.

(6) Teller, E. The crossing of potential surfaces. *J. Phys. Chem.* **1937**, *41*, 109−116.

(7) Horke, D. A.; Li, Q.; Blancafort, L.; Verlet, J. R. R. Ultrafast above-threshold dynamics of the radical anion of a prototypical quinone electron-acceptor. *Nat. Chem.* **2013**, *5*, 711−717.

(8) Bearpark, M. J.; Bernardi, F.; Olivucci, M.; Robb, M. A.; Smith, B. R. Can fulvene S_1 decay be controlled? A CASSCF study with MMVB dynamics. *J. Am. Chem. Soc.* **1996**, *118*, 5254−5260.

(9) Martínez, T. J. Insights for light-driven molecular devices from ab initio multiple spawning excited-state dynamics of organic and biological chromophores. *Acc. Chem. Res.* **2006**, *39*, 119−126.

(10) Li, Q.; Mendive-Tapia, D.; Paterson, M. J.; Migani, A.; Bearpark, M. J.; Robb, M. A.; Blancafort, L. A global picture of the S_1/S_0 conical intersection seam of benzene. *Chem. Phys.* **2010**, *377*, 60−65.

(11) Li, Q.; Migani, A.; Blancafort, L. Wave packet dynamics at an extended seam of conical intersection: mechanism of the light-induced Wolff rearrangement. *J. Phys. Chem. Lett.* **2012**, *3*, 1056−1061.

(12) Cui, G.; Thiel, W. Photoinduced ultrafast Wolff rearrangement: A non-adiabatic dynamics perspective. *Angew. Chem., Int. Ed.* **2013**, *52*, 433−436.

(13) Barbatti, M.; Aquino, A. J. A.; Szymczak, J. J.; Nachtigallova, D.; Hobza, P.; Lischka, H. Relaxation mechanisms of UV-photoexcited DNA and RNA nucleobases. *Proc. Natl. Acad. Sci. U.S.A.* **2010**, *107*, 21453−21458.

(14) Martín, M. E.; Negri, F.; Olivucci, M. Origin, nature, and fate of the fluorescent state of the green fluorescent protein chromophore at the CASPT2//CASSCF resolution. *J. Am. Chem. Soc.* **2004**, *126*, 5452−5464.

(15) Merchán, M.; González-Luque, R.; Climent, T.; Serrano-Andrés, L.; Rodríguez, E.; Reguero, M.; Peláez, D. Unified model for the ultrafast decay of pyrimidine nucleobases. *J. Phys. Chem. B* **2006**, *110*, 26471−26476.

(16) Marian, C. M. A new pathway for the rapid decay of electronically excited adenine. *J. Chem. Phys.* **2005**, *122*, 104314.

(17) Perun, S.; Sobolewski, A. L.; Domcke, W. Ab initio studies on the radiationless decay mechanisms of the lowest excited singlet states of 9H-adenine. *J. Am. Chem. Soc.* **2005**, *127*, 6257−6265.

(18) Blancafort, L. Excited-state potential energy surface for the photophysics of adenine. *J. Am. Chem. Soc.* **2006**, *128*, 210−219.

(19) Conti, I.; Garavelli, M.; Orlandi, G. The different photoisomerization efficiency of azobenzene in the lowest n,π^* and π,π^* singlets: The role of a phantom state. *J. Am. Chem. Soc.* **2008**, *130*, 5216−5230.

(20) Boggio-Pasqua, M.; Ravaglia, M.; Bearpark, M. J.; Garavelli, M.; Robb, M. A. Can diarylethene photochromism be explained by a reaction path alone? A CASSCF study with model MMVB dynamics. *J. Phys. Chem. A* **2003**, *107*, 11139−11152.

(21) Li, Q.; Blancafort, L. A conical intersection model to explain aggregation induced emission in diphenyl dibenzofulvene. *Chem. Commun.* **2013**, *49*, 5966−5968.

(22) Atchity, G. J.; Xantheas, S. S.; Ruedenberg, K. Potential-energy surfaces near intersections. *J. Chem. Phys.* **1991**, *95*, 1862−1876.

(23) Blancafort, L.; Lasorne, B.; Bearpark, M. J.; Worth, G. A.; Robb, M. A. Second-Order Analysis of Conical Intersections: Applications to Photochemistry and Photophysics of Organic Molecules. In *The Jahn-*

DOI: 10.1021/acs.jctc.5b00004
J. Chem. Theory Comput. 2015, 11, 1585−1594

Teller Effect: Fundamentals and Implications for Physics and Chemistry; Köppel, H., Yarkony, D. R., Barentzen, H., Eds.; Springer Series in Chemical Physics, 97; Springer: Heidelberg, Germany, 2009; pp 169−200.
(24) Blancafort, L. Photochemistry and photophysics at extended seams of conical intersection. *ChemPhysChem* **2014**, *15*, 3166−81.
(25) Blancafort, L.; Ogliaro, F.; Olivucci, M.; Robb, M. A.; Bearpark, M. J.; Sinicropi, A. Computational Investigation Of Photochemical Reaction Mechanisms. In *Computational Methods in Photochemistry*; Kutateladze, A. G., Ed.; Molecular and Supramolecular Photochemistry, Taylor & Francis: Boca Raton, FL, 2005; Vol. *13*, pp 31−110.
(26) Manaa, M. R.; Yarkony, D. R. On the intersection of 2 potential-energy surfaces of the same symmetry - systematic characterization using a Lagrangian multiplier constrained procedure. *J. Chem. Phys.* **1993**, *99*, 5251−5256.
(27) Bearpark, M. J.; Robb, M. A.; Schlegel, H. B. A direct method for the location of the lowest energy point on a potential surface crossing. *Chem. Phys. Lett.* **1994**, *223*, 269−274.
(28) Anglada, J. M.; Bofill, J. M. A reduced-restricted-quasi-Newton-Raphson method for locating and optimizing energy crossing points between two potential energy surfaces. *J. Comput. Chem.* **1997**, *18*, 992−1003.
(29) Toniolo, A.; Ben-Nun, M.; Martínez, T. J. Optimization of conical intersections with floating occupation semiempirical configuration interaction wave functions. *J. Phys. Chem. A* **2002**, *106*, 4679−4689.
(30) De Vico, L.; Olivucci, M.; Lindh, R. New general tools for constrained geometry optimizations. *J. Chem. Theory Comput.* **2005**, *1*, 1029−1037.
(31) Muñoz Losa, A.; Martín, M. E.; Galván, I. F.; Aguilar, M. A. Location of conical intersections in solution using a sequential quantum mechanics/molecular dynamics method. *Chem. Phys. Lett.* **2007**, *443*, 76−81.
(32) Levine, B. G.; Coe, J. D.; Martínez, T. J. Optimizing conical intersections without derivative coupling vectors: application to multistate multireference second-order perturbation theory (MS-CASPT2). *J. Phys. Chem. B* **2008**, *112*, 405−413.
(33) Sicilia, F.; Blancafort, L.; Bearpark, M. J.; Robb, M. A. New algorithms for optimizing and linking conical intersection points. *J. Chem. Theory Comput.* **2008**, *4*, 257−266.
(34) Maeda, S.; Ohno, K.; Morokuma, K. Updated branching plane for finding conical intersections without coupling derivative vectors. *J. Chem. Theory Comput.* **2010**, *6*, 1538−1545.
(35) Mori, T.; Nakano, K.; Kato, S. Conical intersections of free energy surfaces in solution: effect of electron correlation on a protonated Schiff base in methanol solution. *J. Chem. Phys.* **2010**, *133*, 064107064107.
(36) Cui, G.; Yang, W. Conical intersections in solution: formulation, algorithm, and implementation with combined quantum mechanics/molecular mechanics method. *J. Chem. Phys.* **2011**, *134*, 204115204115.
(37) Ruiz-Barragan, S.; Robb, M. A.; Blancafort, L. Conical intersection optimization based on a double Newton-Raphson algorithm using composed steps. *J. Chem. Theory Comput.* **2013**, *9*, 1433−1442.
(38) Minezawa, N. Optimizing minimum free-energy crossing points in solution: linear-response free energy/spin-flip density functional theory approach. *J. Chem. Phys.* **2014**, *141*, 164118.
(39) Maseras, F.; Morokuma, K. IMOMM - a new integrated ab-initio plus molecular mechanics geometry optimization scheme of equilibrium structures and transition-states. *J. Comput. Chem.* **1995**, *16*, 1170−1179.
(40) Humbel, S.; Sieber, S.; Morokuma, K. The IMOMO method: Integration of different levels of molecular orbital approximations for geometry optimization of large systems: Test for n-butane conformation and S_N2 reaction: RCl+Cl. *J. Chem. Phys.* **1996**, *105*, 1959−1967.
(41) Svensson, M.; Humbel, S.; Froese, R. D. J.; Matsubara, T.; Sieber, S.; Morokuma, K. ONIOM: a multilayered integrated MO +MM method for geometry optimizations and single point energy predictions. A test for Diels-Alder reactions and $Pt(P(t\text{-}Bu)_3)_2+H_2$ oxidative addition. *J. Phys. Chem.* **1996**, *100*, 19357−19363.
(42) Svensson, M.; Humbel, S.; Morokuma, K. Energetics using the single point IMOMO (integrated molecular orbital plus molecular orbital) calculations: choices of computational levels and model system. *J. Chem. Phys.* **1996**, *105*, 3654−3661.
(43) Dapprich, S.; Komaromi, I.; Byun, K. S.; Morokuma, K.; Frisch, M. J. A new ONIOM implementation in Gaussian98. Part I. The calculation of energies, gradients, vibrational frequencies and electric field derivatives. *J. Mol. Struct. (THEOCHEM)* **1999**, *461*, 1−21.
(44) Vreven, T.; Morokuma, K. On the application of the IMOMO (integrated molecular orbital plus molecular orbital) method. *J. Comput. Chem.* **2000**, *21*, 1419−1432.
(45) Vreven, T.; Morokuma, K. The ONIOM (our own N-layered integrated molecular orbital plus molecular mechanics) method for the first singlet excited (S_1) state photoisomerization path of a retinal protonated Schiff base. *J. Chem. Phys.* **2000**, *113*, 2969−2975.
(46) Chung, L. W.; Hirao, H.; Li, X.; Morokuma, K. The ONIOM method: its foundation and applications to metalloenzymes and photobiology. *WIREs Comput. Mol. Sci.* **2012**, *2*, 327−350.
(47) Bearpark, M. J.; Larkin, S. M.; Vreven, T. Searching for conical intersections of potential energy surfaces with the ONIOM method: application to previtamin D. *J. Phys. Chem. A* **2008**, *112*, 7286−7295.
(48) Rappe, A. K.; Casewit, C. J.; Colwell, K. S.; Goddard, W. A.; Skiff, W. M.; UFF, A. Full periodic table force field for molecular mechanics and molecular dynamics simulations. *J. Am. Chem. Soc.* **1992**, *114*, 10024−10035.
(49) Vreven, T.; Morokuma, K.; Farkas, O.; Schlegel, H. B.; Frisch, M. J. Geometry optimization with QM/MM, ONIOM, and other combined methods. I. Microiterations and constraints. *J. Comput. Chem.* **2003**, *24*, 760−769.
(50) Palmer, I. J.; Ragazos, I. N.; Bernardi, F.; Olivucci, M.; Robb, M. A. An MC-SCF study of the S_1 and S_2 photochemical-reactions of benzene. *J. Am. Chem. Soc.* **1993**, *115*, 673−682.
(51) Olivucci, M.; Ragazos, I. N.; Bernardi, F.; Robb, M. A. A conical intersection mechanism for the photochemistry of butadiene - A MC-SCF study. *J. Am. Chem. Soc.* **1993**, *115*, 3710−3721.
(52) Bernardi, F.; Olivucci, M.; Ragazos, I. N.; Robb, M. A. A new mechanistic scenario for the photochemical transformation of ergosterol - an MC-SCF and MM-VB study. *J. Am. Chem. Soc.* **1992**, *114*, 8211−8220.
(53) Tong, H.; Dong, Y.; Hong, Y.; Haussler, M.; Lam, J. W. Y.; Sung, H. H. Y.; Yu, X.; Sun, J.; Williams, I. D.; Kwok, H. S.; Tang, B. Z. Aggregation-induced emission: effects of molecular structure, solid-state conformation, and morphological packing arrangement on light-emitting behaviors of diphenyldibenzofulvene derivatives. *J. Phys. Chem. C* **2007**, *111*, 2287−2294.
(54) Frisch, M. J.; Trucks, G. W.; Schlegel, H. B.; Scuseria, G. E.; Robb, M. A.; Cheeseman, J. R.; Scalmani, G.; Barone, V.; Mennucci, B.; Petersson, G. A.; Nakatsuji, H.; Caricato, M.; Li, X.; Hratchian, H. P.; Izmaylov, A. F.; Bloino, J.; Zheng, G.; Sonnenberg, J. L.; Hada, M.; Ehara, M.; Toyota, K.; Fukuda, R.; Hasegawa, J.; Ishida, M.; Nakajima, T.; Honda, Y.; Kitao, O.; Nakai, H.; Vreven, T.; Montgomery, J. A., Jr.; Peralta, J. E.; Ogliaro, F.; Bearpark, M. J.; Heyd, J. J.; Brothers, E.; Kudin, K. N.; Staroverov, V. N.; Kobayashi, R.; Normand, J.; Rhagavachari, K.; Rendell, A.; Burant, J. C.; Iyengar, S. S.; Tomasi, J.; Cossi, M.; Rega, N.; Millam, J. M.; Klene, M.; Knox, J. E.; Cross, J. B.; Bakken, V.; Adamo, C.; Jaramillo, J.; Gomperts, R.; Stratmann, R. E.; Yazyev, O.; Austin, A. J.; Cammi, R.; Pomelli, C.; Ochterski, J. W.; Martin, R. L.; Morokuma, K.; Zakrzewski, G.; Voth, G. A.; Salvador, P.; Dannenberg, J. J.; Dapprich, S.; Daniels, A. D.; Farkas, O.; Foresman, J. B.; Ortiz, J. V.; Cioslowski, J.; Fox, D. J. *Gaussian 09*, revision A.02; Gaussian, Inc.: Wallingford, CT, 2009.
(55) Schlegel, H. B. Geometry Optimization: 1. In *Encyclopedia of Computational Chemistry*; Schleyer, P. v. R., Ed. John Wiley & Sons: Chichester, UK, 1998; Vol. 2, pp 1136−1142.

DOI: 10.1021/acs.jctc.5b00004
J. Chem. Theory Comput. 2015, 11, 1585−1594

(56) Sicilia, F.; Blancafort, L.; Bearpark, M. J.; Robb, M. A. Quadratic description of conical intersections: characterization of critical points on the extended seam. *J. Phys. Chem. A* **2007**, *111*, 2182−2192.
(57) Bock, H.; Ruppert, K.; Herdtweck, E.; Herrmann, W. A. Structures of molecules with charge excitation of steric packing. 17. Structural changes on reduction of 9-(diphenylmethylidene)fluorene by sodium metal to sheets of $(R_2O)Na^+$-connected hydrocarbon dianions. *Helv. Chim. Acta* **1992**, *75*, 1816−1824.
(58) Yamamoto, N.; Vreven, T.; Robb, M. A.; Frisch, M. J.; Schlegel, H. B. A direct derivative MC-SCF procedure. *Chem. Phys. Lett.* **1996**, *250*, 373−378.
(59) Li, Q.; Mennucci, B.; Robb, M. A.; Blancafort, L.; Curutchet, C. Polarizable QM/MM multi-configuration self-consistent field approach with state-specific corrections: environment effects on cytosine absorption spectrum. *J. Chem. Theory Comput.* **2015**, DOI: 10.1021/ct5010388.

DOI: 10.1021/acs.jctc.5b00004
J. Chem. Theory Comput. 2015, 11, 1585−1594